HEALTH AND MEDICINE

Engineered algae: A novel oxygen-generating system for effective treatment of hypoxic cancer

Yue Qiao[1,2]*, Fei Yang[1]*, Tingting Xie[2]*, Zhen Du[2], Danni Zhong[2], Yuchen Qi[2], Yangyang Li[2], Wanlin Li[2,3], Zhimin Lu[2], Jianghong Rao[3], Yi Sun[2,4]†, Min Zhou[1,2,4,5]†

Microalgae, a naturally present unicellular microorganism, can undergo light photosynthesis and have been used in biofuels, nutrition, etc. Here, we report that engineered live microalgae can be delivered to hypoxic tumor regions to increase local oxygen levels and resensitize resistant cancer cells to both radio- and phototherapies. We demonstrate that the hypoxic environment in tumors is markedly improved by in situ–generated oxygen through microalgae-mediated photosynthesis, resulting in notably radiotherapeutic efficacy. Furthermore, the chlorophyll from microalgae produces reactive oxygen species during laser irradiation, further augmenting the photosensitizing effect and enhancing tumor cell apoptosis. Thus, the sequential combination of oxygen-generating algae system with radio- and phototherapies has the potential to create an innovative treatment strategy to improve the outcome of cancer management. Together, our findings demonstrate a novel approach that leverages the products of photosynthesis for treatment of tumors and provide proof-of-concept evidence for future development of algae-enhanced radio- and photodynamic therapy.

INTRODUCTION

Rapidly growing solid tumors inevitably encounter hypoxia because of outgrowth of the cell mass over vessels (*1*, *2*). Local hypoxia in tumors is a serious impediment for cancer therapies, leading to greatly reduced effectiveness, particularly for radiotherapy (RT) (*3*, *4*) and photodynamic therapy (PDT) (*5*, *6*), in which oxygen is involved in the process of cell killing. Improving oxygenation in hypoxic tumor regions and overcoming hypoxia should substantially enhance the PDT/RT efficacy. Thus, reoxygenation of hypoxic tumors would be an effective approach to overcome hypoxia-based resistance to conventional cancer therapies (*7*–*9*).

The in situ generation of oxygen in tumor with nanocarriers has been attempted to increase local oxygen in the hypoxic region for enhancement of therapeutic efficacy (*10*–*15*). However, this approach has very limited translational value, mainly because most of the administered nanocarriers were captured by the mononuclear phagocyte system (MPS) in the liver and spleen, leading to only ~2% of the total administered dose being deposited in tumor (*16*). High uptake of nanocarriers in major organs increases the risk of systemic toxicity, thereby preventing their clinical application (*17*–*19*).

In nature, microalgae have evolved an elaborate oxygenic photosynthesis system with the capability of highly efficient photocatalyzed O_2 generation (*20*). Microalgae have been used in various applications including biofuels, nutrition, foods, feeds, biofertilizers, pollution control, bioremediation, and high-value bioactive compounds that exploit their photosynthetic ability (*21*–*23*). *Chlorella vulgaris* is a unicellular microalga that can generate O_2 by photosynthesis (*24*). Because of their abundant sources, economic price, and uniformity in structure, algae have traditionally been used as a research model for development of new food sources and, more recently, for enhanced production of biofuels using CO_2 as a carbon source (*25*). It is worth noting that *Chlorella* is capable of reducing endotoxemia in digestive diseases (*26*) and enhancing host defenses against peritonitis (*27*) without side effects. Moreover, *C. vulgaris* contains a large concentration of chlorophyll, which absorbs light across a broad wavelength spectrum and thus enables photosynthesis at a range of wavelengths; this feature could be used for PDT to generate reactive oxygen species (ROS) under 650-nm irradiation (*28*, *29*). Also, the primary product of disintegrated algae, chlorophyll, has no genetic side effects in mammalian cells, including chromosomal breakages (*30*), and it can limit the bioavailability of carcinogens in human uptake (*31*) with no obvious induction of immunoreaction. However, whether and how algae can be used as an oxygen source for the treatment of hypoxic tumors in combination with radio- and phototherapies have never been previously investigated.

Here, we report an innovative method to overcome tumor hypoxia by in situ generation of O_2 using a natural photosynthetic system based on engineered *C. vulgaris*. We first engineered the red blood cell membrane (RBCM), and used it as an efficient strategy for modification of the algal surface to reduce macrophage uptake and systemic clearance of the algae (*32*–*35*) in order to exploit algal metabolic activity for enhanced delivery of *C. vulgaris* to tumor tissues. We demonstrated that the RBCM-engineered algae (abbreviated as RBCM-Algae) successfully delivered to tumor tissues generated O_2 in situ under red light–induced photosynthesis to increase tissue oxygenation and alleviate tumor hypoxia, leading to improved RT. The subsequent release of chlorophyll from microalgae by laser irradiation produced ROS to further confer PDT, resulting in further enhanced cancer cell killing (Fig. 1A).

RESULTS

Bioengineering and characterization of RBCM-Algae

C. vulgaris (algae) have uniform spherical morphology with an average diameter of 2.1 ± .0.8 μm (Fig. 1B). The RBCM-Algae were

[1]Eye Center & Key Laboratory of Cancer Prevention and Intervention, MOE, The Second Affiliated Hospital, Zhejiang University School of Medicine, Hangzhou 310029, China. [2]Institute of Translational Medicine and The Cancer Institute of the Second Affiliated Hospital, Zhejiang University School of Medicine, Hangzhou 310029, China. [3]Department of Radiology and Bio-X, Stanford University, Stanford, CA 94305, USA. [4]Division of Radiation and Cancer Biology, Department of Radiation Oncology 94305, University of Michigan, Ann Arbor, MI 48109, USA. [5]State Key Laboratory of Modern Optical Instrumentations, Zhejiang University, Hangzhou 310058, China.
*These authors contributed equally to this work.
†Corresponding author. Email: zhoum@zju.edu.cn (M.Z.); yisun@zju.edu.cn (Y.S.)

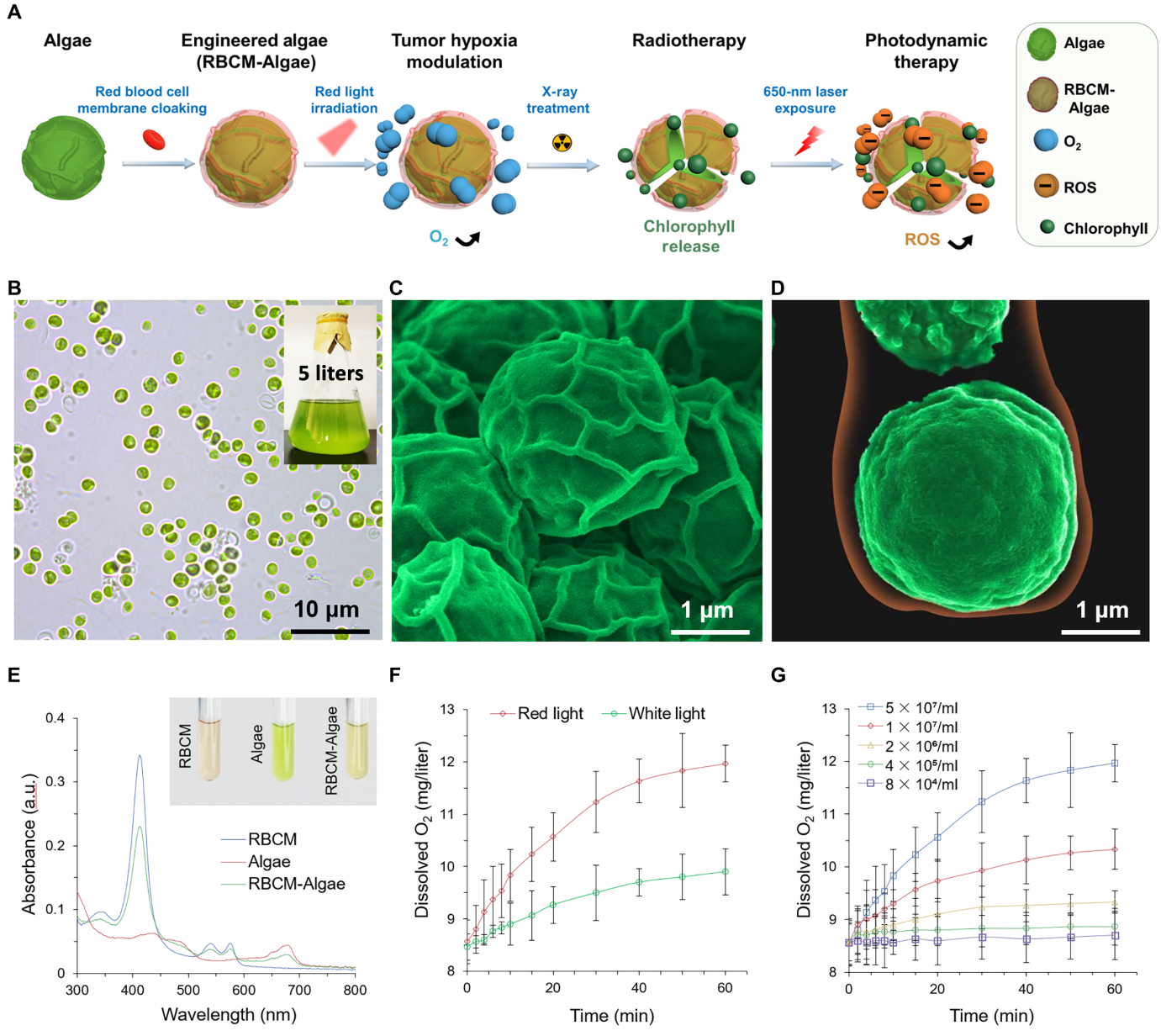

Fig. 1. Characterization of the RBCM-Algae biosystem. (**A**) Illustrative description of engineered processes and treatments. (**B**) Photograph of algae (inset, large-scale preparation of algae). Pseudocolor SEM images of algae (**C**) and RBCM-coated algae (**D**). (**E**) Optical absorption of the algae (inset, photographs). (**F**) Oxygenation of the RBCM-Algae under white/red light irradiation. (**G**) Concentration-dependent oxygenation of the RBCM-Algae. Data are means ± SD, $n = 3$ for each group. a.u., arbitrary units.

prepared by cloaking algal cells with RBCM isolated from RBC. The microstructure of algae alone, or with RBCM coating as a unilamellar membrane coating over the algae, was readily visualized by scanning electron microscopy (SEM) and transmission electron microscopy (Fig. 1, C and D, and fig. S1, A to F). Physicochemical characterizations revealed that the RBCM-Algae were approximately 3 μm in diameter, larger than uncloaked algae and RBCM alone (fig. S1G). The optical absorbance and fluorescence properties of the RBCM-Algae were similar to those of the uncloaked algae (Fig. 1E and fig. S1H). To further demonstrate that the RBCM was cloaking the algal cells, we performed sodium dodecyl sulfate–polyacrylamide gel electrophoresis (SDS-PAGE) to measure the protein composition of RBCM and RBCM-Algae. The migration pattern of various proteins was nearly identical in the two samples, confirming that algae were coated by RBCM (fig. S1I). Collectively, these results indicated that algae can be cloaked with the membrane of red blood cells (RBC) to generate RBCM-Algae.

RBCM-Algae have oxygenation ability

Algae under red light (660-nm light-emitting diode light) show higher photosynthesis activity than under natural white light (*32*). Upon exposure to the red light, RBCM-Algae (5×10^7 algae/ml) produced a high amount of O_2 within 60 min at a level of 12.1 mg/liter of oxygen concentration in both time- and concentration-dependent manners (Fig. 1, F and G), a higher rate than that observed in white light (9.9 mg/liter). Also, the oxygenation ability of RBCM-Algae

showed no obvious differences from that of uncloaked algae (fig. S2, A and B). Further, the oxygenation ability of RBCM-Algae did not display a noticeable decline under red light with penetration depths of 2 and 4 mm (fig. S2C). Under storage conditions of 4°C, there was no notable change in oxygenation ability of RBCM-Algae (5×10^7 cells/ml) within 6 days (fig. S2, D and E). These results suggest that RBCM-Algae can release oxygen to the surrounding environment as effectively as uncloaked algae.

Evaluation of RBCM-Algae in cell culture settings

We next characterized the RBCM-Algae as a multifunctional agent in a cell culture setting by examining its vitality, cytotoxicity, alleviation of hypoxia, improvement of radiation therapy efficacy, and reinforcement of photodynamic therapeutic capability. RBCM-Algae showed high survival rates (all above 80%) over a long-term test period (fig. S3A) or variation temperature test (fig. S3B). Embryonic 4T1 murine breast cancer cells exhibited excellent tolerance to RBCM-Algae under physiological conditions. Analyses by methyl thiazolyl tetrazolium (MTT) assay showed that RBCM-Algae, even at a high concentration of 5×10^7 cells/ml, did not affect survival of 4T1 cancer cells, human SKOV3 ovarian cancer cells, human kidney human embryonic kidney (HEK) 293 cells, HepG2 cells, fibroblast, Jurkat T cells (fig. S3, C to H), or murine J774 macrophages (fig. S3I). In addition, RBCM-Algae did not induce secretion of interleukin-1β (IL-1β) from J774 macrophages (fig. S3J). Hemolytic test was performed, and RBCM-Algae did not induce obvious hemolysis below concentration of 5×10^7 cells/ml (fig. S3, K and L).

Given that RBCM-Algae can actively undergo photosynthesis under physiological conditions, the ability of RBCM-Algae to modulate cellular hypoxic conditions was assessed. The corresponding mechanism of hypoxic radiosensitization by RBCM-Algae was explored by probing the intracellular O_2 level using an oxygen-sensitive $[Ru(dpp)_3]Cl_2$ indicator. As expected, the red fluorescence of hypoxia probe was quenched in the cells under hypoxic conditions and incubated with RBCM-Algae in a time-dependent manner with a peak at 2 hours after exposure to red light for 60 min (Fig. 2A), indicating a great improvement of hypoxia arising from the efficient O_2 release and diffusion through cells. These results indicated that RBCM-Algae counteract hypoxia by its excellent oxygenation ability under exposure to red light.

We next used a clonogenic assay to evaluate radiation-induced apoptosis after alleviation of cellular hypoxia by RBCM-Algae. As expected, breast 4T1 cancer cells grown under hypoxia conditions were substantially more resistant to irradiation than those grown under normoxia conditions. Notably, RBCM-Algae largely eliminated the resistance of cancer cells under hypoxic conditions to radiation (Fig. 2B and fig. S4A). These results indicated that RBCM-Algae–based oxygenation via photosynthesis sensitizes hypoxic cancer cells to radiation.

We then used immunofluorescence staining to assess the x-ray irradiation–induced DNA damage reflected by γ-H2AX, a biomarker of double-strand DNA breaks. Consistent with the clonogenic assay, cancer cells had much less damaged DNA under hypoxic conditions than under normoxic conditions upon radiation. RBCM-Algae treatment significantly increased DNA damage in the hypoxic cancer cells to a similar level to that in the normoxic cells (Fig. 2, C and D). Thus, the improved oxygen supply released from the RBCM-Algae induces more DNA damage to sensitize cancer cells to radiation.

We found that the external x-ray irradiation could break the RBCM-Algae (fig. S4B) and demonstrated a dose-dependent response (Fig. 2E). Most of the intercellular chlorophyll was released after the x-ray treatment (Fig. 2F) and then could be internalized by the surrounding cancer cells (Fig. 2G). Because RBCM-Algae have the ability to release chlorophyll, a photosensitizer, we used calcein acetoxymethyl (AM)/propidium iodide (PI) staining to investigate the potential effect of RBCM-Algae on PDT. As expected, the combination of RBCM-Algae with laser remarkably induced apoptosis, as reflected by much stronger red fluorescence intensity (apoptotic cells) compared with each individual treatment (Fig. 2H and fig. S4C). The effect was in a manner dependent on laser power density. To investigate the mechanism underlying the observed effect, we measured ROS production using dichlorofluorescein diacetate (DCFH-DA), a green fluorescent ROS indicator. Upon 660-nm laser irradiation ($0.6\ W/cm^2$, 5 min), the fluorescence intensity of DCFH-DA from the RBCM-Algae–treated 4T1 cells was much stronger than those in the cells with each individual treatment (fig. S4, D to F). These results indicated that RBCM-Algae increase ROS production under red light production, thereby enhancing PDT efficacy.

RBCM-Algae increase O_2 in tumor tissues

We cloaked RBCM on the surface of algae to protect it from the clearance from many MPS organs. It is also known that the ample natural markers (such as CD47, sialic acid, and glycan) on the membrane of RBCs contribute to the avoidance of immunogenic clearance of RBC-associated formulations (*32*, *36*). Thus, we expected that RBCM-Algae should have an extended life span and increased stability during in vivo circulation, which would improve tumor delivery efficacy owing to excellent addressability and biocompatibility of the RBCM. To test this hypothesis, we intravenously injected RBCM-Algae into the mice bearing subcutaneous 4T1 tumors, which were examined by an in vivo imaging system. The fluorescence signals (chlorophyll of the algae has fluorescence signal) in the tumor were detected at 0.25 hour after injection of RBCM-Algae, reached a peak at 2 hours, and then gradually decreased to the basal level at 24 hours (Fig. 3, A and B), demonstrating the optimized time window for oxygenation. As compared with native algae without modifications, RBCM-Algae showed much higher accumulation in tumors (fig. S5, A and B). It is known that fluorescence imaging has limited tissue penetration (less than 1 cm) and low resolution (*37*–*39*). We collected tissues and performed ex vivo fluorescence imaging for further verification. Compared with a majority of normal tissues, the tumor tissues had the highest uptake of RBCM-Algae, as evidenced by the fluorescence signals of major organs at various time points in the biodistribution study (Fig. 3, C and D). Together with excretion analysis performed by the fluorescence signals of urine and feces, our results indicated that RBCM-Algae could undergo both renal and hepatobiliary clearance routes after intravenous injection (fig. S6). SEM analyses revealed a large number of RBCM-Algae in the tumor tissues after intravenous injection at the 2-hour time point (Fig. 3E and fig. S5C). Furthermore, immunohistological analysis of tumor slices demonstrated that RBCM-Algae (red signals) in tissues collected 2 hours after administration (Fig. 3F) colocalized with tumor microvascular walls (endothelial marker CD31 staining, green signals). We also found the RBCM-Algae in the tumor microvessels (white arrow in Fig. 3F and fig. S5D). These data demonstrated that the RBCM-Algae could reach the tumor tissue after intravenous injection.

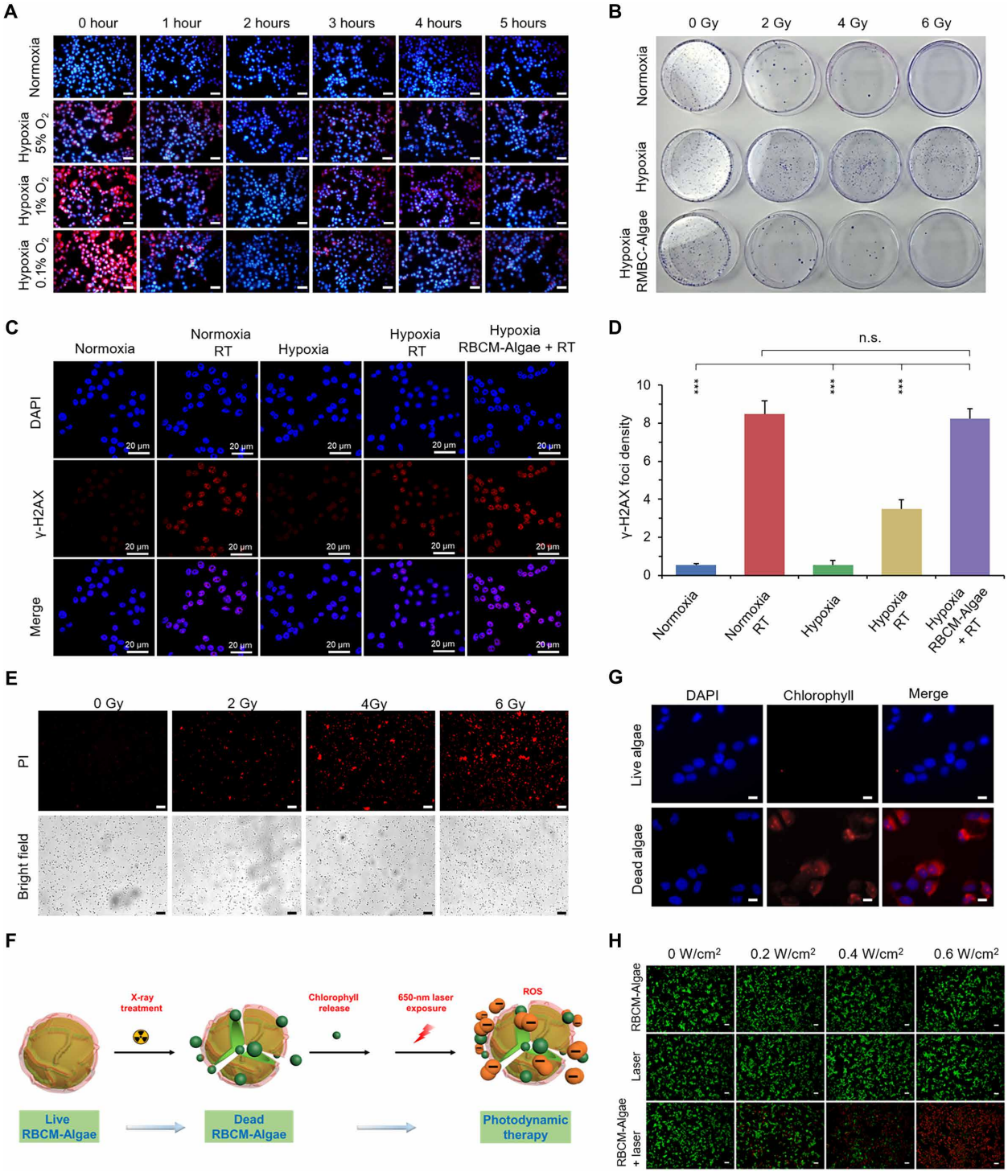

Fig. 2. Engineered algae could increase oxygen, improve radiotherapeutic effect, release chlorophyll, and induce PDT. (**A**) Confocal fluorescence images showing increased intracellular O_2 level after treatment with RBCM-Algae in hypoxia incubation with hypoxia probe $[Ru(dpp)_3]Cl_2$. Scale bars, 40 μm. (**B**) Clonogenic assay of 4T1 cells in vitro showing increased sensibility of RT. More cancer cells were killed by RBCM-Algae–mediated x-ray irradiation. (**C**) Cell DNA damage evaluated by γ-H2AX foci. (**D**) The corresponding quantitative analysis of the number of foci per cell. More DNA damages and cancer cell–killing effects were found for the hypoxia cancer cells by the RBCM-Algae under red light irradiation (6000 lux, 2 hours). (**E**) Live/dead staining of the algae showed that a large number of the dead algae were found after the x-ray treatment. Scale bars, 50 μm. X-ray treatment could kill the algae, and the internal chlorophyll of the algae was released after the treatment. (**F**) Scheme of the process of the RBCM-Algae after x-ray treatment. (**G**) Fluorescence images of the 4T1 cancer cells after the incubation of the released chlorophyll, demonstrating the internalization of the chlorophyll in the cancer cells [4′,6-diamidino-2-phenylindole (DAPI), blue; chlorophyll, red]. Scale bars, 5 μm. (**H**) Representative confocal fluorescence microscopy images of live/dead staining assay of 4T1 cells via calcein-AM (green, viable cells) and PI (red, dead cells) staining. Scale bars, 100 μm. Data are means ± SD, $n = 3$, Student's two-tailed t test, not significant (n.s.) $P \geq 0.05$; ***$P < 0.001$. Photo credit for (B): M.Z., Zhejiang University.

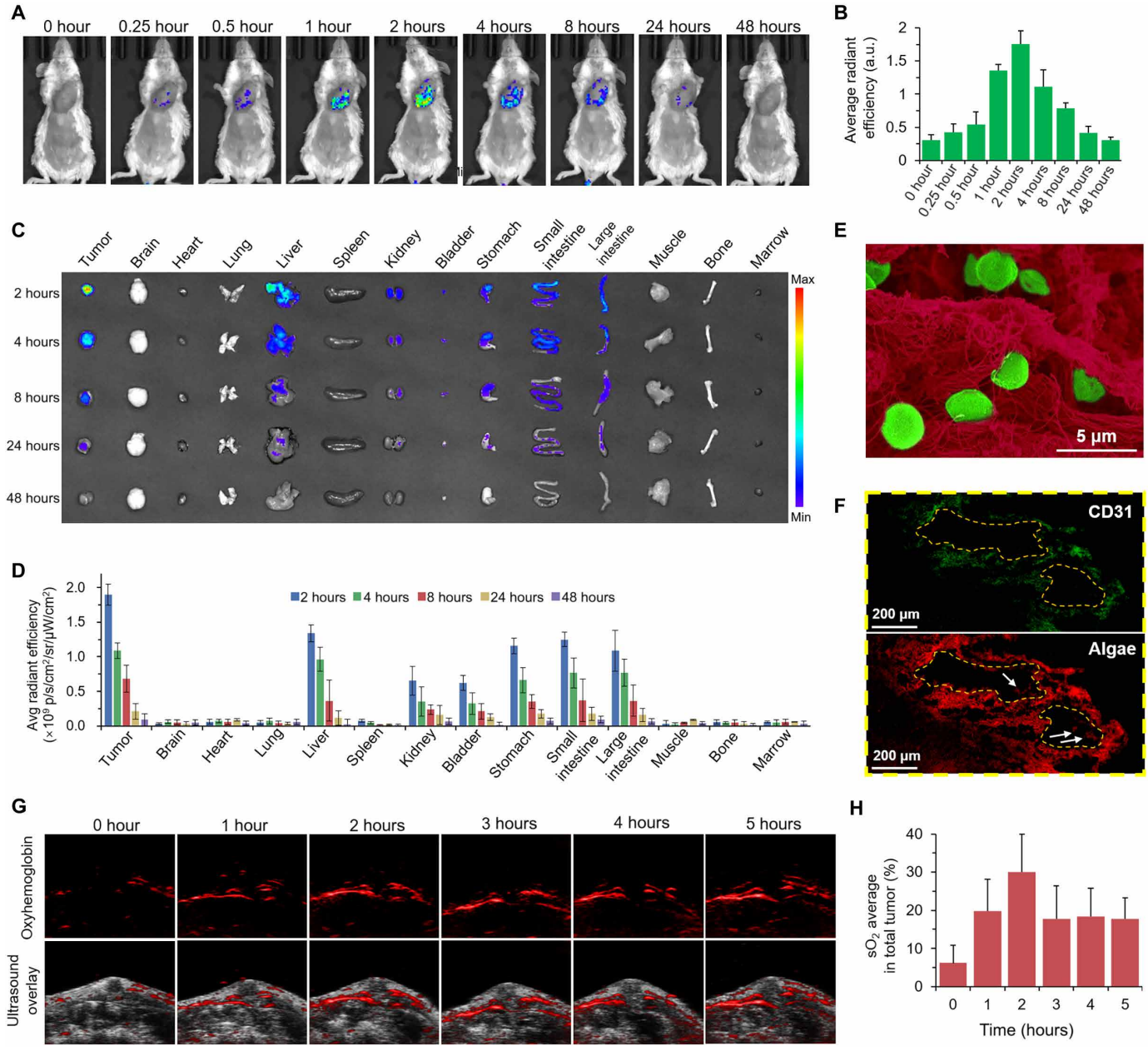

Fig. 3. Engineered algae could efficiently reach tumor site after intravenous injection and improve oxyhemoglobin. In vivo fluorescence imaging (**A**) of the mice and the quantitative analysis (**B**), ex vivo imaging (**C**), and the quantitative analysis (**D**) of the tumor uptake after intravenous injection of RBCM-Algae in 4T1 tumor-bearing mice. (**E**) Pseudocolor SEM images of tumor tissues; RBCM-Algae (green) were found in the tumor (red) 2 hours after intravenous injection of RBCM-Algae. (**F**) CD31 staining for tumor microvessels (green). The red signals are RBCM-Algae. (**G**) In vivo PA images of oxygen hemoglobin in 4T1 tumor at different time points after intravenous administration of RBCM-Algae and (**H**) the corresponding sO_2 quantitative analysis. Data are means ± SD, $n = 3$.

We next assessed the effect of RBCM-Algae on oxygen saturation within orthotopic 4T1 breast tumor with a small animal photoacoustic (PA) imaging system following the intravenous injection of RBCM-Algae. PA imaging measures vasculature saturated O_2 (sO_2) by the optical absorption of oxygenated hemoglobin, which is directly correlated with the change of O_2 concentration in the blood (*40*). As shown in Fig. 3 (G and H), the injected RBCM-Algae significantly increased the signal intensity of blood oxygen saturation in the tumor region from 6.2 to 30.0% within 2 hours; the signal intensity then began to decrease due to the diffusion of RBCM-Algae and O_2. Accordingly, PA signal intensity of deoxygenated hemoglobin was continuously declining during the first 2 hours, demonstrating the decrease in tumor hypoxia (fig. S5E). On the basis of this result, we decided to deliver x-ray irradiation to local tumors at 2 hours after injection of RBCM-Algae, which is the peak time point for blood oxygen saturation.

RBCM-Algae sensitize tumor to irradiation

We next determined whether RBCM-Algae would sensitize tumor cells to radiation using two xenografted models derived from 4T1 breast tumor and SKOV3 ovarian tumor cells. Compared with treatments with radiation or RBCM-Algae alone, the combination of RBCM-Algae with x-ray irradiation significantly suppressed the tumor growth derived from 4T1 breast tumor cells (fig. S7, A to D) and extended mice survival (fig. S7E). The tumor weights were approximately sixfold ($P < 0.001$), threefold ($P < 0.001$), and fivefold ($P < 0.001$) lighter than those treated with phosphate-buffered saline (PBS) control, RT, and RBCM-Algae, respectively (fig. S7D). The histopathologic analyses, including hematoxylin and eosin (H&E) and terminal deoxynucleotidyl transferase–mediated deoxyuridine triphosphate nick end labeling (TUNEL), of the resected tumors revealed that combination treatment remarkably enhanced apoptosis (fig. S7, F and G). Similar radiosensitization of SKOV3 cell–derived tumor by RBCM-Algae was observed (fig. S8). These results indicated that RBCM-Algae increase O_2 in tumor tissues and sensitize tumor to irradiation.

RBCM-Algae mediate both radiation and photodynamic therapies to enhance therapeutic effect

We next assessed the efficacy of RBCM-Algae in enhancing RT and PDT in mice inoculated with 4T1 breast cancer cells (1×10^6 cells) (detailed experimental designs are shown in fig. S9). When the size of tumors reached 100 to 150 mm^3 in volume (about 7 days), RBCM-Algae (2×10^6 cells) were injected directly into tumors, followed by exposure to 660-nm red light (5 min). The tumors were sequentially irradiated by x-ray [2 gray (Gy)] and the 660-nm laser (0.5 W/cm^2, 10 min). Local intratumoral administration of RBCM-Algae in the combination of RT-PDT resulted in complete tumor elimination, while the control of RBCM-Algae with just RT or PDT yielded about 80% tumor suppression (fig. S9). Survival analysis showed that 90% of mice receiving triple-combination therapy were still alive after 40 days of the experimental period, while all mice in the other experimental groups died, although the combination of RBCM-Algae with RT or PDT notably extended mouse life span (fig. S9G).

We repeated this experiment by systemic administration of RBCM-Algae via intravenous injection. While combined treatment of RBCM-Algae with RT or PDT caused partial tumor growth inhibition, the triple combination produced further enhanced suppression of tumor growth, as reflected by the lowest tumor growth rate and smallest tumor size at the end of the experiment (Fig. 4, A to E). In addition, triple-combination therapy was well tolerated in mice, as reflected by normal body weight (fig. S10A), normal ranges of various blood tests (fig. S10B), and normal morphology of H&E-stained major organs (fig. S10C). Immunohistochemistry staining of tumors showed that tumors receiving triple-combination therapy had the lowest tumor cell density (H&E), reduced proliferation reflected by Ki-67 expression, reduced angiogenesis reflected by endothelial marker CD31 expression, and robust apoptosis reflected by cleaved caspase-3 (Fig. 4F). Together, these findings indicated that RBCM-Algae sensitize RT-PDT therapy in vivo by inhibiting tumor cell proliferation and inducing apoptosis.

Molecular mechanism underlying RBCM-Algae–mediated abrogation of hypoxia-dependent radioresistance

To elucidate the molecular mechanism underlying the antihypoxia action of RBCM-Algae, we determined early molecular events following the triple-combination therapy as outlined in Fig. 5A. We found significantly increased levels of ROS, peaking at 5.1 to 5.3 hours in the tumors, following sequential treatments of the x-ray irradiation and laser PDT; this finding revealed an effective ROS production by RBCM-Algae (Fig. 5B). Given that hypoxia often induces hypoxia-inducible factor 1 (HIF-1) transcription factor to transactivate a variety of signal molecules, including vascular endothelial growth factor (VEGF) to increase angiogenesis and promote tumor growth (*41*), we used immunohistochemical staining and Western blotting to examine the dynamic change of HIF1α, VEGF, and proliferation and apoptosis of tumor cells (Fig. 5, D to F). The triple combination of RBCM-Algae + RT + laser significantly reduced levels of HIF1α and VEGF (Fig. 5, D and E) inversely correlated with the time frame of ROS production by oxygenation (Fig. 5C). Specifically, the levels of HIF1α and VEGF decreased at 2 hours post–RBCM-Algae intravenous injection, reached to the lowest levels at 5.3 to 8 hours, and returned to the high levels at 48 hours, while the levels of CD31, Ki-67, and cleaved caspase-3 remained unchanged at the first 6 hours, followed by remarkable decrease in CD31 and Ki-67 expression or increase in cleaved caspase-3 until 7 days (Fig. 5, D and E). Thus, the triple RBCM-Algae + RT + laser combination treatment effectively induced tumor regression by inhibiting angiogenesis and proliferation and inducing apoptosis.

In many types of solid tumors, hypoxia is a common characteristic, arising from an imbalance between increased oxygen consumption driven by rapid cancer cell proliferation and inadequate oxygen supply owing to defective tumor vascularization (*42*). Hypoxia is often associated with cancer progression and resistance to therapeutics (*43*, *44*). It is well established that hypoxia up-regulates HIF1α, which independently promotes radioresistance. HIF1α is an instrumental mediator of hypoxia signaling and plays a predominant role in the hypoxic response through the transactivation of downstream target genes, including VEGF (*45*). Under hypoxic conditions, HIF1α is stabilized and permits the activation of genes essential for cellular adaptation to low-oxygen conditions. VEGF is a major regulator of angiogenesis, which promotes endothelial cell migration toward a hypoxic area (*46*). During hypoxia, HIF-1 binds the regulatory region of the VEGF gene, inducing its transcription and initiating its expression, which in turn stimulates the development of new blood vessels to enrich tumor cells with oxygen for their growth (*47*). Following RT, the lack of oxygen reduces the ROS production and attenuates DNA damage in cancer cells, thus preventing cancer cell killing. Thus, improvement of local hypoxia conditions by any means likely enhances therapeutic efficacy by radiation and is, therefore, in high demand.

DISCUSSION

In this study, we found that algae can effectively produce oxygen in our experimental system (Fig. 1). We further demonstrated that RBCM-engineered algae can be effectively delivered to tumors via either intratumoral or intravenous injection to improve local oxygen loading and effectively sensitize cancer cells to RT-PDT therapies in two xenograft tumor models (Figs. 2 to 4). Mechanistically, we showed that RBCM-Algae–based triple-combination therapies indeed improve local oxygen concentrations, as evidenced by reduced levels of HIF1α and VEGF, two commonly used hypoxic biomarkers, and trigger large amounts of ROS production, leading to reduced proliferation and increased apoptosis (Fig. 5) and tumor regression (Fig. 4). In

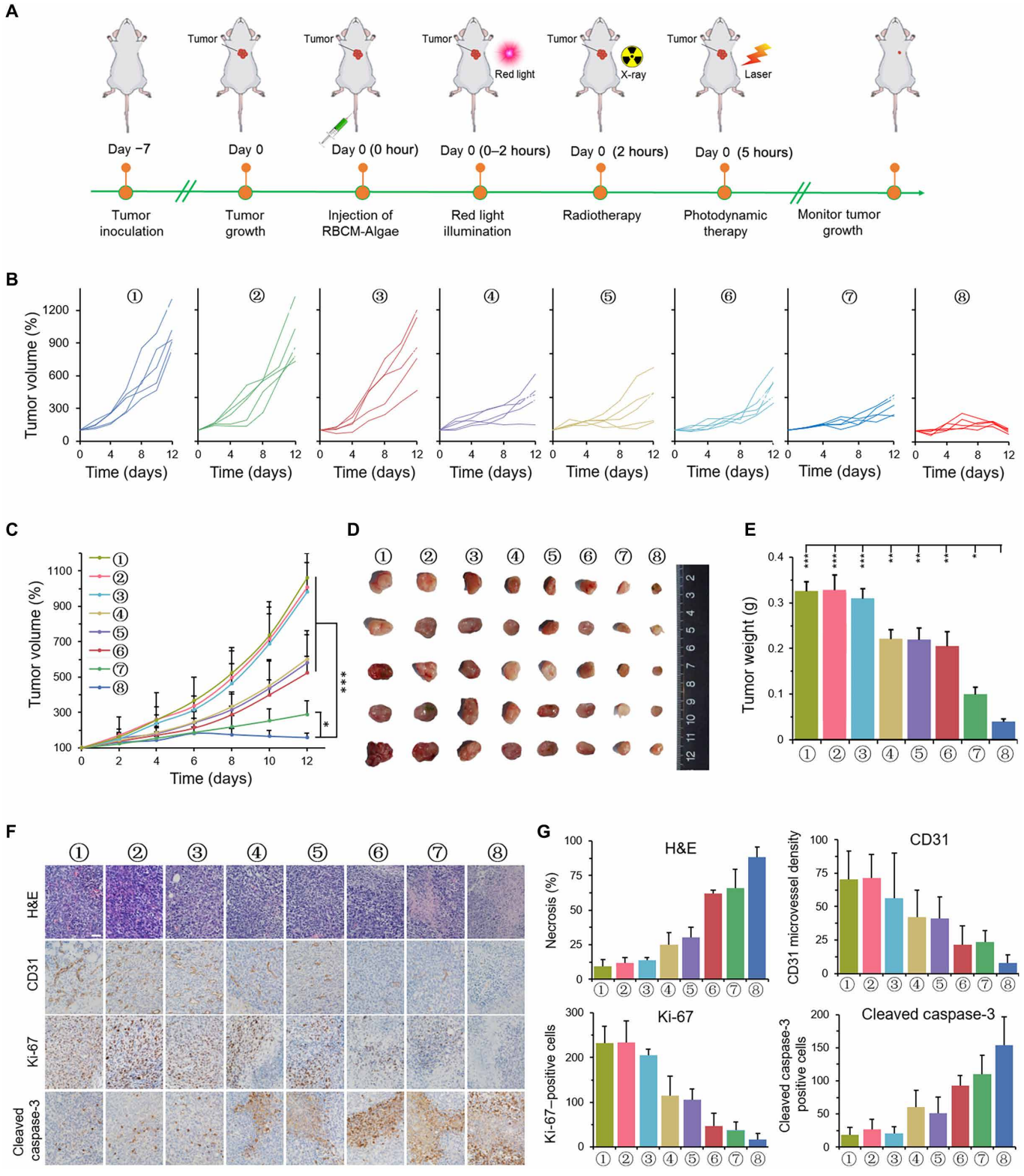

Fig. 4. Engineered algae-mediated RT, and PDT can inhibit efficiently the tumor growth (4T1 breast cancer model) after intravenous injection. (**A**) Scheme illustrating treatments. (**B**) Tumor growth curves of individual mice. (**C**) Average tumor growth curves of all the groups. Photographs (**D**) and weight (**E**) of the tumors collected from the 4T1 tumor–bearing mice of each group (day 12). (**F** and **G**) Representative H&E, CD31, Ki-67, and cleaved caspase-3 staining of tumor sections from the tumor tissues in different treatment groups (day 12) and corresponding immunohistochemical index quantitative analysis. Treatments: 1, control; 2, laser alone; 3, RBCM-Algae alone; 4, x-ray irradiation (RT) alone; 5, RT + laser; 6, RBCM-Algae + laser; 7, RBCM-Algae + RT; and 8, RBCM-Algae + RT + laser. Data are means ± SD, $n = 5$, Student's two-tailed t test, not significant $P \geq 0.05$; *$P < 0.05$; **$P < 0.01$; ***$P < 0.001$.

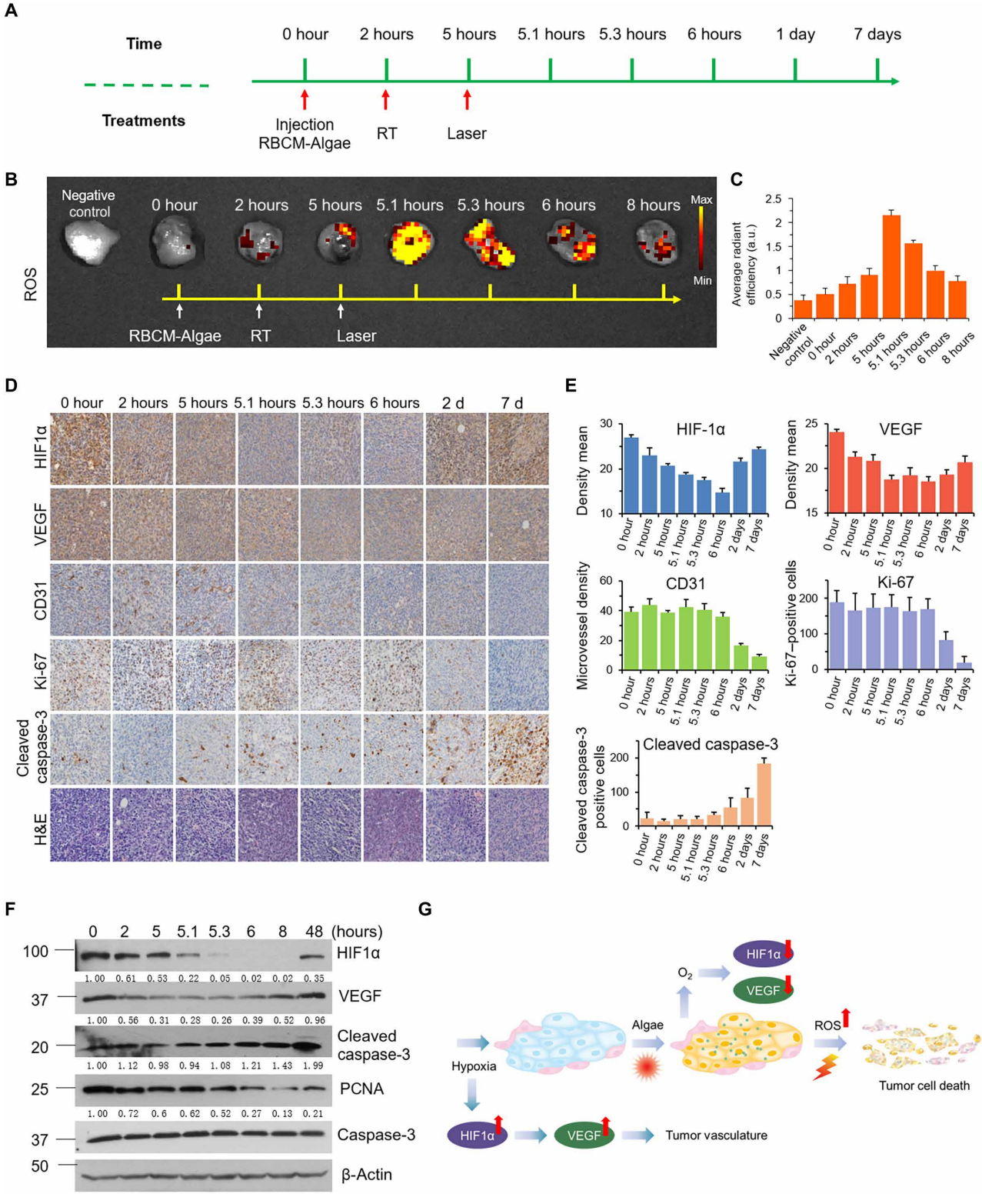

Fig. 5. Mechanism of the treatments, RBCM-Algae decrease the protein level of HIF1α and VEGF and promotes cell apoptosis and necrosis. (**A**) Tumor collection timetable from the process of in vivo anticancer PBS biosystem therapy. (**B**) Bioluminescence imaging and (**C**) the corresponding quantitative analysis of tumor tissues that were stained with ROS probe (DCFH). (**D**) Representative HIF1α, CD31, Ki-67, cleaved caspase-3, and H&E staining of tumor section from in situ 4T1 tumor–bearing mice of RBCM-Algae treated by RBCM-Algae + RT + laser and the corresponding immunohistochemical index quantitative analysis (**E**). (**F**) Immunoblotting of HIF1α, VEGF, cleaved caspase-3, proliferating cell nuclear antigen (PCNA), and caspase-3 protein level from 4T1 tumor–bearing mice of the RBCM-Algae + RT + laser group and the corresponding quantitative analysis. (**G**) Possible mechanism of the RBCM-Algae–mediated combination therapy. Data are means ± SD, $n = 3$.

summary, our study reveals that algae-radiation-laser combination therapy effectively suppresses tumor growth via blockage of the HIF1α/VEGF axis to inhibit angiogenesis and proliferation and induce apoptosis (Fig. 5G).

Our work presents a naturally plentiful, living photosynthetic organism, algae with its engineered form RBCM-Algae, which can modulate the tumor hypoxia microenvironment and eliminate cancer cells by combination of RT and photodynamic therapies without causing apparent toxicity. We efficiently delivered the algae to the tumor by cloaking of RBCM on the surface of the living biosystem. We identified that the oxygenation in the tumor environment by in situ photosynthesis of algae could relieve hypoxia and improve the cancer cells' sensitivity to radiation treatment. We also found that PDT could further enhance cancer cell apoptosis by the innate chlorophyll of the algae under laser irradiation without introducing any photosensitizers. The triple combination of RBCM-Algae with RT and PDT synergistically enhanced cancer cell apoptosis, leading to tumor regression in mice. Systemic administration of RBCM-Algae exhibited a superior anticancer efficacy in terms of both tumor regression and mouse survival rate. Hence, this naturally living biomaterial-based therapy provides an attractive approach for efficient cancer treatment. The preliminary investigation confirmed the RBCM-Algae biosafety in vivo, indicating that algae inhibit tumor growth with minimal toxicity at the tested dose. Nevertheless, more systematic studies, such as long-term toxicity and immunecompatibility studies, are still necessary before translation to clinical application.

MATERIALS AND METHODS

Synthesis of RBCM-Algae

The algae (GY-H4 *C. vulgaris*) were purchased by Shanghai Guangyu Biological Technology, China. The RBCs were collected by centrifugation at 3000 rpm for 10 min, removing the supernatant and washing three times with ice-cold PBS [4°C (pH 7.4)] until a transparent supernatant appeared. The obtained precipitate was then dissolved in ice-cold tris-HCl solution [0.01 M (pH 7.4)] with a volume ratio of 1:40 at 4°C for 2 hours to extract RBCM. Afterward, the obtained samples were purified by centrifugation at 9000 rpm for 20 min to remove possible aggregates in the supernatants. The same procedure was repeated three times until a clear solution without visible RBC was observed. Last, PBS [0.01 M (pH 7.4)] was added to dissolve the precipitate and stored at −20°C until further use. To introduce RBCM coating, RBCM was collected via cryogenic ultrasonication for 10 to 20 min until the mixture turned transparent. The as-prepared RBCM was then suspended in algae (GY-H4 *C. vulgaris*) with a volume ratio of 1:1, mixed under gentle magnetic stirring overnight at 4°C, and subsequently collected by centrifugation at 3000 rpm for 10 min to obtain RBCM-Algae for later use.

RBCM protein characterization using SDS-PAGE

The successful synthesis of RBCM-Algae was confirmed by the SDS-PAGE method. In a typical procedure, the RBCM, algae, and RBCM-Algae protein were prepared in SDS sample buffer and further determined by the bicinchoninic acid (BCA) assay kit (Beyotime, China). The RBCM, algae, and RBCM-Algae proteins with equal mass amounts were solubilized and resolved into the wells on a polyacrylamide gel. The samples were then run on a 10% SDS-PAGE gel using tris-glycine-SDS buffer as running buffer in the Mini-PROTEAN Tetra System (Bio-Rad, CA, USA) at 300 mA for 2 hours based on the manufacturer's instructions. Afterward, the samples were run at 120 V for 1 hour, and the resulting polyacrylamide gel was stained in Coomassie R-250 for 1 hour, followed with distaining overnight using a solution consisting of 10% ethanol and 7.5% acetic acid. The protein signals were measured by the enhanced chemiluminescence method using the ChemiDoc MP gel imaging system (Bio-Rad, CA, USA).

RBCM-Algae viability measurements

Briefly, freshly prepared RBCM-Algae were maintained into a conical flask in an illumination incubator at 27°C. At the same incubation time during the period daily, an equal volume of RBCM-Algae was seeded into 96-well plates, and the viability of RBCM-Algae was determined by examining the absorbance at 600 nm using the Universal Microplate Reader (Molecular Devices SpectraMax M5, USA). Later, PI was used for dead cell staining, which was recorded using a Zeiss microscope (Olympus IX71, Japan) under bright field and fluorescence. The built-in threshold plugin of ImageJ was used to count the number of live and dead cells and calculate the relative ratio. The live/dead assays were performed in triplicate, and three images were obtained for each well.

Influence of temperature on viabilities of RBCM-Algae

For measurement of temperature-mediated viabilities of RBCM-Algae, 5×10^7/ml of RBCM-Algae were cultured in various ambient temperatures of 27° or 37°C with red light illumination (4600 lux). Then, an equivalent number of RBCM-Algae were collected into 96-well plates at each preset time point of 2, 4, 6, 8, and 10 hours after incubation for further evaluation.

DCFH-DA staining

Intratumor production of ROS was measured by oxidation of DCFH-DA. DCFH-DA is a nonpolar compound that can readily diffuse into cells, where it is hydrolyzed to the nonfluorescent polar derivative, DCFH, and thereby trapped within cells. If DCFH is oxidized, it turns into the highly fluorescent DCF. After the mice were euthanized, tumors were incubated in the dark for 30 min at 37°C with 10 μM DCFH-DA (Biyuntian, #S0033, China). After incubation, the tumors were washed with PBS and analyzed within 30 min by in vivo imaging system (PerkinElmer, USA). The specific fluorescence signals corresponding to DCHF-DA were collected at 525 nm.

Characterization of RBCM-Algae

General characterization of the RBCM-Algae was performed by dynamic light scattering (Zetasizer Nano-ZS90 Malvern, USA), fluorescence and ultraviolet/visible spectroscopy (Shimadzu UV-2600, Japan), and field emission SEM (Hitachi SU-70, Japan) and high-resolution transmission electron microscopy (Tecnai F20, FEI, USA).

O_2 production of RBCM-Algae

To investigate the oxygen release profile in real time, an equal volume of algae and RBCM-Algae, with a dose of 30 ml separately at a final concentration of 10^6/ml, was added into the cuvette, which was then subjected to white or red light sources at a power density of 4600 lux. A portable dissolved oxygen meter was applied to record the oxygen concentrations at selected time intervals after irradiation. The

dissolved oxygen concentration was subsequently calculated. To test the concentration-dependent effects, 30 ml of freshly prepared RBCM-Algae of a series of concentrations was placed in a 50-ml tube, which was irradiated with red light at an output power of 4600 lux. After treatment, the oxygen production efficiency was quantified at different time points. Stability analysis was performed at the 4°C storage condition for 2 weeks, and the penetration depth assay used chicken breast block (2 and 4 mm). Three replicates were done for each concentration.

In vitro cytotoxicity assay

The standard thiazolyltetrazolium (MTT, Sigma-Aldrich, USA) assay was carried out to determine the cytotoxicity of the synthesized RBMC-Algae using various cell lines (4T1, SKOV3, HEK293, HepG2, fibroblast, Jurkat T, and J774 cells) before evaluation of the therapeutic effect. Briefly, cells were seeded in a 96-well flat-bottom plate at a density of 1×10^5 cells per well and incubated in varying concentrations of RBMC-Algae for at least 24 hours. Thereafter, the medium of the cells was refreshed with PBS followed by the addition of 20 μl of MTT solution (5 mg/ml) to each well for further incubation at 37°C for an additional 4 hours for the assay. The culture medium was collected, and cytokine concentrations were assessed using a mouse IL-1β enzyme-linked immunosorbent assay (ELISA) kit (BioLegend, USA) following the manufacturer's instructions.

For the hemolysis assay, mice blood (5 ml) was centrifuged (1500 rpm, 15 min) and rinsed with PBS three times to collect RBC. Diluted RBC suspension was mixed with four times the volume of RBCM-Algae dispersion (in PBS) at various concentrations (5×10^7, 1×10^7, and 2×10^6 cells/ml). PBS and deionized H_2O are the negative and positive controls, respectively. After incubation (RT, 4 hours), all the mixed suspension was centrifuged (12,000 rpm, 15 min), and the 450-nm optical density was determined via a microplate reader (Molecular Devices, USA).

Animals and tumor models

All experiments involving animals were in accordance with the guidelines of the Institutional Animal Care and Use Committee of Zhejiang University and were performed under protocols approved by this committee. Female Balb/c mice (6 weeks of age) were purchased from Shanghai Slac Laboratory Animal Co. Ltd. The orthotopic breast cancer tumor model was established in the Balb/c mice by injection of 1×10^6 4T1 cells [American Type Culture Collection (ATCC), Manassas, VA] suspended in 50 μl of PBS medium onto the mammary fat pads of each mouse.

Biodistribution

For biodistribution of RBCM-Algae after intravenous injection, 6-week-old female BALB/c mice bearing orthotopic 4T1 breast tumors ($n = 3$) were administered a tail vein injection of freshly prepared RBCM-Algae (1×10^6/ml, 150 μl per mouse). Major organs and tissues including tumor, brain, heart, lung, liver, spleen, kidney, bladder, stomach, small intestine, large intestine, muscle, bone, and marrow were removed at 0 min, 15 min, 30 min, 1 hour, 2 hours, 4 hours, 8 hours, 24 hours, and 48 hours after injection and observed using an in vivo imaging system (PerkinElmer, USA) with parameters of excitation wave of 465 nm and emission wave of Cy5.5. The bioluminescence activity uptake by RBCM-Algae was measured, wherein the critical aggregation concentration of RBCM-Algae intravenously was determined from the average radiant efficiency, which was further quantified using the software. Collected urine and feces were also analyzed by the same protocol.

Intratumoral injection therapy

For in vivo intratumoral injection assay, the 4T1 breast cancer–bearing mice were randomly assigned to eight groups (five mice per group) when the tumor sizes reached about 100 mm^3 (2 weeks after inoculation): group 1, control; group 2, laser alone; group 3, RBCM-Algae alone; group 4, x-ray irradiation (RT) alone; group 5, RT plus laser; group 6, RBCM-Algae plus laser; group 7, RBCM-Algae plus RT; group 8, RBCM-Algae plus RT plus laser. For combination treatment, the tumors in group 8 received standardized procedures as follows: 4T1 breast cancer–bearing mice were intratumorally injected with RBCM-Algae (1×10^6/ml, 50 μl per mouse) by four uniformly distributed injections. After treatment, the animals were anesthetized with intraperitoneal injection of chloral hydrate (4%, 150 μl) before subjecting to x-ray irradiation (RT, 6 Gy) for 3 hours. Then, continuous 2% isoflurane at a flow rate of 2 liters/min was delivered to the 4T1 tumors followed by PDT (650-nm laser, 10 min). After various treatments, the animals were imaged on day 0 (time of inoculation) and every 2 days thereafter. Tumor sizes and body weight were also monitored at baseline and every 2 days for 2 weeks, with their lengths and widths measured by a digital caliper and the tumor volume calculated according to the following formula: (tumor length) × (tumor width)^2/2, which were further quantified using the software program ImageJ to monitor tumor growth. At the 12th day of therapy, all mice were euthanized, and tumor tissues from each group of mice were dissected, weighed, and processed for histological evaluation. The treatments for the other groups were set as follows: The mice in group 1 were untreated. The tumors in groups 2 and 4 received laser irradiation and x-ray irradiation alone, respectively. The tumors in group 3 were intratumorally injected with RBCM-Algae alone. The tumors in group 5 were irradiated with laser illumination combined with x-ray. The tumors in groups 6 and 7 were intratumorally injected with RBCM-Algae combined with laser or x-ray, respectively. The tumors in group 8 were intratumorally injected with RBCM-Algae combined with x-ray and laser treatments.

Intravenous injection therapy

Mice bearing 4T1 breast tumors were prepared as described above. All the mice were also assigned into eight groups ($n = 5$ per group). The treatments for the other groups were set as follows: The mice in group 1 were untreated. The tumors in groups 2 and 4 received laser irradiation and x-ray irradiation alone, respectively. The tumors in group 3 were intravenously injected with RBCM-Algae alone (1×10^6/ml, 150 μl per mouse). The tumors in group 5 were irradiated with laser illumination combined with x-ray. The tumors in groups 6 and 7 were intravenously injected with RBCM-Algae (1×10^6/ml, 150 μl per mouse) combined with laser or x-ray, respectively. The tumors in group 8 received intravenous injection of RBCM-Algae (1×10^6/ml, 150 μl per mouse) combined with x-ray irradiation and PDT. Mouse body weight was measured every 2 days. The tumors were allowed to grow for 12 days, which were imaged and weighed on day 0 (time of inoculation) and every 2 days afterward. After the last administration at day 12, the mice were euthanized after cardiac puncture to collect tumors for weighing and blood samples for hematologic and clinical chemistry analysis to assess the safety profile of intravenous administration. Biochemical analyses were performed

by collecting serum from the blood in a coagulation tube containing a separation tube. Moreover, the major organs of mice, including heart, liver, spleen, kidney, and lung in each group, were removed, weighed, cryosectioned, and stained with H&E for further histological examinations, which were observed using virtual slide microscopy (Olympus VS120, Japan).

The ovarian cancer tumor model was established in the Balb/c mice by subcutaneous injection of 5×10^6 SKOV3 cells (ATCC, VA) suspended in 50 μl of PBS medium onto the thigh of each mouse. All the mice were randomly assigned into four groups ($n = 5$ per group). The treatments for the other groups were set as follows: The mice in group 1 were untreated. The tumors in group 2 received x-ray irradiation alone. The tumors in group 3 were intravenously injected with RBCM-Algae alone (1×10^6/ml, 150 μl per mouse). The tumors in group 4 were intravenously injected with RBCM-Algae (1×10^6/ml, 150 μl per mouse) combined with x-ray. Mouse body weight was measured every 2 days. The tumors were allowed to grow for 10 days, which were measured on day 0 (time of inoculation) and every 2 days afterward. On day 10, the mice were euthanized after cardiac puncture to collect tumors for histopathological analysis.

Histology/immunohistochemistry/image analysis/quantification

When the mice were euthanized, subcutaneous tumors were removed and fixed in 10% neutral buffered formalin and then embedded in paraffin. Paraffin-embedded tumor sections (4 μm) were cut using a microtome (Leica RM2235, Germany) and mounted on slides. H&E-stained tumor sections were stained using standard histological techniques. For immunohistochemical analyses for HIF1α, VEGF, CD31, Ki-67, and cleaved caspase-3 staining, the sections were stained with corresponding antibodies. Last, slices were photographed with a Virtual slide microscope (Olympus VS120, Japan). The photographs were analyzed with the Image-Pro Plus 6.0 software (Media Cybernetics Inc., Silver Spring, MD, USA).

Quantification of the immunohistochemical staining of HIF1α and VEGF proteins in tumors was evaluated on the basis of the ratio and intensity of the staining. Three random fields in each section were calculated. The measurement parameters collected by Image-Pro Plus 6.0 included density means, area sum, and intensity of distribution (IOD). The optical density was counted, and the area of interest was set through the following: hue, 0~30; intensity, 0~255; saturation, 0~255; next, the image was converted to a grayscale image, and the values were counted. The density mean, equal to (IOD SUM)/area, represented the concentration of specific protein per unit area. For tumor vascularization analysis, the three regions with the highest density of CD31-positive microvessels were selected at low power (×100) and quantified at high magnification (×400). Microvessels with a clearly defined lumen or with a well-defined linear vessel shape were included in the counts. The final microvessel density for each case was the mean of the number of vessels counted in the three hot spots that were scored. For Ki-67 or cleaved caspase-3 quantification, three images per one tumor from each treatment group were manually analyzed with IPP software. The positive cells were counted per field as the proliferation or apoptosis index.

Statistical analysis

All statistical analyses were performed using the SPSS software package (SPSS Inc., USA). All error bars used in this study are means ± SD of at the least three independent experiments. Statistically significant P values are indicated in figures and/or legends as $^{***}P < 0.001$; $^{**}P < 0.01$; $^{*}P < 0.05$.

SUPPLEMENTARY MATERIALS

Supplementary material for this article is available at http://advances.sciencemag.org/cgi/content/full/6/21/eaba5996/DC1

View/request a protocol for this paper from *Bio-protocol*.

REFERENCES AND NOTES

1. J. A. Bertout, S. A. Patel, M. C. Simon, The impact of O_2 availability on human cancer. *Nat. Rev. Cancer* **8**, 967–975 (2008).
2. J. B. West, Physiological effects of chronic hypoxia. *N. Engl. J. Med.* **376**, 1965–1971 (2017).
3. H. E. Barker, J. T. Paget, A. A. Khan, K. J. Harrington, The tumor microenvironment after radiotherapy: mechanisms of resistance and recurrence. *Nat. Rev. Cancer* **15**, 409–425 (2015).
4. D. Schaue, W. H. McBride, Opportunities and challenges of radiotherapy for treating cancer. *Nat. Rev. Clin. Oncol.* **12**, 527–540 (2015).
5. A. Casas, G. Di Venosa, T. Hasan, A. Batlle, Mechanisms of resistance to photodynamic therapy. *Curr. Med. Chem.* **18**, 2486–2515 (2011).
6. A. L. Maas, S. L. Carter, E. P. Wileyto, J. Miller, M. Yuan, G. Yu, A. C. Durham, T. M. Busch, Tumor vascular microenvironment determines responsiveness to photodynamic therapy. *Cancer Res.* **72**, 2079–2088 (2012).
7. J. L. Rummer, D. J. McKenzie, A. Innocenti, C. T. Supuran, C. J. Brauner, Root Effect hemoglobin may have evolved to enhance general tissue oxygen delivery. *Science* **340**, 1327–1329 (2013).
8. S. M. Hatfield, J. Kjaergaard, D. Lukashev, T. H. Schreiber, B. Belikoff, R. Abbott, S. Sethumadhavan, P. Philbrook, K. Ko, R. Cannici, M. Thayer, S. Rodig, J. L. Kutok, E. K. Jackson, B. Karger, E. R. Podack, A. Ohta, M. V. Sitkovsky, Immunological mechanisms of the antitumor effects of supplemental oxygenation. *Sci. Transl. Med.* **7**, 277ra30 (2015).
9. S. Xu, X. Zhu, C. Zhang, W. Huang, Y. Zhou, D. Yan, Oxygen and Pt(II) self-generating conjugate for synergistic photo-chemo therapy of hypoxic tumor. *Nat. Commun.* **9**, 2053 (2018).
10. H. Chen, J. Tian, W. He, Z. Guo, H_2O_2-activatable and O_2-evolving nanoparticles for highly efficient and selective photodynamic therapy against hypoxic tumor cells. *J. Am. Chem. Soc.* **137**, 1539–1547 (2015).
11. W. Fan, W. Bu, B. Shen, Q. He, Z. Cui, Y. Liu, X. Zheng, K. Zhao, J. Shi, Intelligent MnO_2 Nanosheets anchored with upconversion nanoprobes for concurrent pH-/H_2O_2-responsive UCL imaging and cxygen-elevated synergetic therapy. *Adv. Mater.* **27**, 4155–4161 (2015).
12. C. Chen, X. Ni, S. Jia, Y. Liang, X. Wu, D. Kong, D. Ding, Massively evoking immunogenic cell death by focused mitochondrial oxidative stress using an AIE luminogen with a twisted molecular structure. *Adv. Mater.* **31**, 01904914 (2019).
13. X. Song, L. Feng, C. Liang, K. Yang, Z. Liu, Ultrasound triggered tumor oxygenation with oxygen-shuttle nanoperfluorocarbon to overcome hypoxia-associated resistance in cancer therapies. *Nano Lett.* **16**, 6145–6153 (2016).
14. J. Zhuang, M. Ying, K. Spiekermann, M. Holay, Y. Zhang, F. Chen, H. Gong, J. H. Lee, W. Gao, R. H. Fang, L. Zhang, Biomimetic nanoemulsions for oxygen delivery in vivo. *Adv. Mater.* **30**, e1804693 (2018).
15. C. Chen, H. Ou, R. Liu, D. Ding, Regulating the photophysical property of organic/polymer optical agents for promoted cancer phototheranostics. *Adv. Mater.* **31**, 2018063314 (2019).
16. S. Wilhelm, A. J. Tavares, Q. Dai, S. Ohta, J. Audet, H. F. Dvorak, W. C. W. Chan, Analysis of nanoparticle delivery to tumors. *Nat. Rev. Mater.* **1**, 16014 (2016).
17. S. Singh, A. Sharma, G. P. Robertson, Realizing the clinical potential of cancer nanotechnology by minimizing toxicologic and targeted delivery concerns. *Cancer Res.* **72**, 5663–5668 (2012).
18. D. Rosenblum, N. Joshi, W. Tao, J. M. Karp, D. Peer, Progress and challenges towards targeted delivery of cancer therapeutics. *Nat. Commun.* **9**, 1410 (2018).
19. S.-m. Park, A. Aalipour, O. Vermesh, J. H. Yu, S. S. Gambhir, Towards clinically translatable in vivo nanodiagnostics. *Nat. Rev. Mater.* **2**, 17014 (2017).
20. R. H. Wijffels, M. J. Barbosa, An outlook on microalgal biofuels. *Science* **329**, 796–799 (2010).
21. Y. Chisti, Biodiesel from microalgae. *Biotechnol. Adv.* **25**, 294–306 (2007).
22. D. R. Georgianna, S. P. Mayfield, Exploiting diversity and synthetic biology for the production of algal biofuels. *Nature* **488**, 329–335 (2012).
23. S. C. Pierobon, X. Cheng, P. J. Graham, B. Nguyen, E. G. Karakolis, D. Sinton, Emerging microalgae technology: A review. *Sustain. Ener. Fuels* **2**, 13–38 (2018).

24. J. Liu, F. Chen, Biology and industrial applications of chlorella: Advances and prospects, in *Microalgae Biotechnology* (Posten C, Chen SF) (2016).
25. Y. Panahi, B. Darvishi, N. Jowzi, F. Beiraghdar, A. Sahebkar, Chlorella vulgaris: a multifunctional dietary supplement with diverse medicinal properties. *Curr. Pharm. Des.* **22**, 164–173 (2016).
26. A. Bedirli, M. Kerem, E. Ofluoglu, B. Salman, H. Katircioglu, N. Bedirli, D. Yilmazer, M. Alper, H. Pasaoglu, Administration of *Chlorella* sp. microalgae reduces endotoxemia, intestinal oxidative stress and bacterial translocation in experimental biliary obstruction. *Clin. Nutr.* **28**, 674–678 (2009).
27. K. Tanaka, T. Koga, F. Konishi, M. Nakamura, M. Mitsuyama, K. Himeno, K. Nomoto, augmentation of host defense by a unicellular green alga, *Chlorella vulgaris*, to *Escherichia Coli* infection. *Infect. Immun.* **53**, 267–271 (1986).
28. B. H. Song, D. H. Lee, B. C. Kim, S. H. Ku, E. J. Park, I. H. Kwon, K. H. Kim, K. J. Kim, Photodynamic therapy using chlorophyll-a in the treatment of acne vulgaris: A randomized, single-blind, split-face study. *J. Am. Acad. Dermatol.* **71**, 764–771 (2014).
29. M. Chu, H. Li, Q. Wu, F. Wo, D. Shi, Pluronic-encapsulated natural chlorophyll nanocomposites for in vivo cancer imaging and photothermal/photodynamic therapies. *Biomaterials* **35**, 8357–8373 (2014).
30. I. Gomaa, S. E. Ali, T. A. El-Tayeb, M. H. Abdel-kader, Chlorophyll derivative mediated PDT versus methotrexate: An in vitro study using MCF-7 cells. *Photodiagn. Photodyn. Ther.* **9**, 362–368 (2012).
31. C. Jubert, J. Mata, G. Bench, R. Dashwood, C. Pereira, W. Tracewell, K. Turteltaub, D. Williams, G. Bailey, Effects of chlorophyll and chlorophyllin on low-dose aflatoxin B_1 pharmacokinetics in human volunteers. *Cancer Prev. Res.* **2**, 1015–1022 (2009).
32. C. M. Hu, L. Zhang, S. Aryal, C. Cheung, R. H. Fang, L. Zhang, Erythrocyte membrane-camouflaged polymeric nanoparticles as a biomimetic delivery platform. *Proc. Natl. Acad. Sci. U.S.A.* **108**, 10980–10985 (2011).
33. N. Mohandas, P. G. Gallagher, Red cell membrane: past, present, and future. *Blood* **112**, 3939–3948 (2008).
34. W. Gao, L. Zhang, Engineering red-blood-cell-membrane-coated nanoparticles for broad biomedical applications. *AIChE J* **61**, 738–746 (2015).
35. R. H. Fang, A. V. Kroll, W. Gao, L. Zhang, Cell membrane coating nanotechnology. *Adv. Mater.* **30**, e1706759 (2018).
36. C. Ash, M. Dubec, K. Donne, T. Bashford, Effect of wavelength and beam width on penetration in light-tissue interaction using computational methods. *Lasers Med. Sci.* **32**, 1909–1918 (2017).
37. V. Koo, P. W. Hamilton, K. Williamson, Non-invasive in vivo imaging in small animal research. *Cell. Oncol.* **28**, 127–139 (2006).
38. L. Arms, D. W. Smith, J. Flynn, W. Palmer, A. Martin, A. Woldu, S. Hua, Advantages and limitations of current techniques for analyzing the biodistribution of nanoparticles. *Front. Pharmacol.* **9**, 802 (2018).
39. A.-L. Robson, P. C. Dastoor, J. Flynn, W. Palmer, A. Martin, D. W. Smith, A. Woldu, S. Hua, Advantages and limitations of current imaging techniques for characterizing liposome morphology. *Front. Pharmacol.* **9**, 80 (2018).
40. H. F. Zhang, K. Maslov, G. Stoica, L. V. Wang, Functional photoacoustic microscopy for high-resolution and noninvasive in vivo imaging. *Nat. Biotechnol.* **24**, 848–851 (2006).
41. S. Movafagh, S. Crook, K. Vo, Regulation of hypoxia-inducible gactor-1a by reactive oxygen species : New developments in an old febate. *J. Cell. Biochem.* **116**, 696–703 (2015).
42. A. J. Majmundar, W. J. Wong, M. C. Simon, Hypoxia-inducible gactors and the response to hypoxic stress. *Mol. Cell* **40**, 294–309 (2010).
43. I. B. Barsoum, C. A. Smallwood, D. R. Siemens, C. H. Graham, A Mechanism of hypoxia-mediated escape from adaptive immunity in cancer cells. *Cancer Res.* **74**, 665–674 (2014).
44. G. N. Masoud, W. Li, HIF-1α pathway: Role, regulation and intervention for cancer therapy. *Acta Pharm. Sin. B* **5**, 378–389 (2015).
45. C. W. Pugh, P. J. Ratcliffe, Regulation of angiogenesis by hypoxia: Role of the HIF system. *Nat. Med.* **9**, 677–684 (2003).
46. N. Suzuki, K. Gradin, L. Poellinger, M. Yamamoto, Regulation of hypoxia-inducible gene expression after HIF activation. *Exp. Cell Res.* **356**, 182–186 (2017).
47. V. L. Dengler, M. D. Galbraith, J. M. Espinosa, Transcriptional regulation by hypoxia inducible factors. *Crit. Rev. Biochem. Mol. Biol.* **49**, 1–15 (2014).

Acknowledgments

Funding: We acknowledge support from the National Key Research and Development Program of China (2018YFC0115701 to M.Z. and 2016YFA0501800 to Y.S.) and the National Natural Science Foundation of China (nos. 81671748 and 81971667). **Author contributions:** M.Z. and Y.S. conceived the project and designed the experiments. Y. Qiao, F.Y., T.X., D.Z., Y. Qi, Y.L., and W.L. performed the experiments and collected and analyzed the data. M.Z., Y.S., Z.L., and J.R. wrote the manuscript. All authors discussed the results and reviewed the manuscript. **Competing interests:** The authors declare that they have no competing interests. **Data and materials availability:** All data needed to evaluate the conclusions in the paper are present in the paper and/or the Supplementary Materials. Additional data related to this paper may be requested from the authors.

Submitted 17 December 2019
Accepted 10 March 2020
Published 20 May 2020
10.1126/sciadv.aba5996

Citation: Y. Qiao, F. Yang, T. Xie, Z. Du, D. Zhong, Y. Qi, Y. Li, W. Li, Z. Lu, J. Rao, Y. Sun, M. Zhou, Engineered algae: A novel oxygen-generating system for effective treatment of hypoxic cancer. *Sci. Adv.* **6**, eaba5996 (2020).